Vol. 590: 227–245, 2018
https://doi.org/10.3354/meps12451

MARINE ECOLOGY PROGRESS SERIES
Mar Ecol Prog Ser

Published March 12

Foraging hotspots of common and roseate terns: the influence of tidal currents, bathymetry, and prey density

Samuel S. Urmy[1,2,*], Joseph D. Warren[1]

[1]School of Marine and Atmospheric Sciences, Stony Brook University, 239 Montauk Hwy, Southampton, NY 11968, USA

[2]*Present address:* Monterey Bay Aquarium Research Institute, 7700 Sandholdt Rd, Moss Landing, CA 95039, USA

ABSTRACT: Foraging seabirds face significant challenges because the distribution of their prey is often patchy and unpredictable. On the other hand, some environmental features do provide more predictable foraging habitats. Successful foragers presumably use both consistent and flexible strategies. However, our understanding of this balance is limited, because simultaneous high-resolution measurements of prey and predator distributions are rarely available. We used a marine radar to map flocks of common terns *Sterna hirundo* and roseate terns *S. dougallii* near their breeding colony on Great Gull Island, New York, USA, in 2014 and 2015. We also surveyed the terns' prey, and tidal currents, using acoustic instruments on small boats. Feeding flocks formed most often in areas where water accelerated over shallow topography. These locations were consistent from one tidal cycle to the next, although flocks did not always form there. A spatial generalized linear model for flock density explained 45% of the deviance in their observed distribution. The mean prey density was not significantly different under flocks than elsewhere, and there were no detectable spatial trends in the prey field. Our results show that terns rely on the physical action of tidal currents to make prey available near the surface, and that the spatial and temporal predictability of this process may be more important to them than the absolute density of the prey. These findings quantify important features of tern foraging habitat, and may prove useful for planning human activities (e.g. offshore wind energy facilities) to reduce their impacts on terns.

KEY WORDS: Acoustics · Marine predator · Physical-biological coupling · Radar · Seabird

INTRODUCTION

Large marine predators such as seabirds face unique challenges when foraging. The ocean is large, lacks obvious visible landmarks, and is composed of a turbulent fluid that transmits visible light poorly. Prey such as fish, squid, and large zooplankton are also mobile, and their distributions are often patchy (Haury et al. 1978, Schneider & Piatt 1986, Hunt et al. 1999). Much of the interest in seabird foraging has focused on their ability to find food in what is thought to be a highly unpredictable environment. There is substantial evidence, however, that the marine environment may not be as unpredictable to seabirds as it appears to humans (Weimerskirch 2007). Telemetry studies have shown that many seabirds repeatedly visit a few well-defined foraging areas (Becker et al. 1993, Irons 1998). These foraging areas may be associated with hydrographic fronts (Decker & Hunt 1996, Hunt et al. 1996, Zamon et al. 2014) or eddies (Godø et al. 2012). Closer to shore, foraging hotspots are often found in places where tidal currents interact with bathymetry, such as humps (Thorne & Read 2013), islands (Johnston et al. 2005), canyons (Warren et al. 2009), shallow sills (Kinder et al. 1983, Hunt & Harrison 1990), and tidal channels or races (Zamon 2003). Slight differences in tidal flow can even lead to the partitioning of habitat between closely related species on very fine spatial scales (Hunt et al. 1998). Most marine predators probably exploit consistent

*Corresponding author: sam.urmy@gmail.com

structures such as these, and we are unlikely to understand their foraging behaviors without first understanding these subtle features of their habitat.

Tidal currents have long been recognized as important for some seabirds, but the mechanisms by which they facilitate foraging are not always well understood. Current velocities and prey densities cannot always be mapped at high resolution, and even when they are, the favorability of these locations is too often attributed to vaguely defined processes such as 'upwelling' or 'prey concentration'. In fact, there are several specific physical processes which could make tidal races good locations to forage. Flow over shallow bathymetry could force deeper prey to within the near-surface diving range of birds. Enhanced turbulent mixing could break up schools, bring prey to the surface by turbulent diffusion, or disorient small prey, making them easier for birds to capture. Finally, accelerated flow through a channel could simply allow birds to search a large volume of water without having to fly a great distance. Knowing which of these processes are at work would allow us to better predict and identify important foraging areas for seabirds. As more areas are considered for the development of offshore infrastructure such as wind farms, the ability to predict foraging areas could be valuable for minimizing their adverse impacts on seabirds.

Two species of seabirds for which these concerns are relevant are common terns *Sterna hirundo* and roseate terns *S. dougallii*. While common terns are abundant, roseate terns are listed as endangered under the United States Endangered Species Act (USFWS 1998). The 2 species are closely related, having diverged only 4 million years ago (Bridge et al. 2005). Both are piscivorous, capturing prey during shallow plunge dives from the air. Roseate terns in the Northwest Atlantic tend to be specialist predators of sand eels (also called sand lance *Ammodytes americanus*), while common terns consume a wider variety of fishes (Safina et al. 1990, Shealer & Kress 1994, Rock et al. 2007b). There is some evidence that common terns feed more often in dense flocks, while roseate terns are specialized to dispersed foraging on shoals and drift lines, perhaps limiting their habitat relative to common terns (Duffy 1986, Safina 1990). Despite these differences, radio tracking at a mixed-species tern colony off Nova Scotia, Canada, showed that the shallow-water foraging areas of common and roseate terns mostly overlapped (Rock et al. 2007a,b). Maximum dive depths are estimated at 2 m for roseate and 0.5 m for common terns (Cabot & Nisbet 2013), limiting them to prey in the uppermost portion of the water column. As a result, they are reliant on other processes bringing prey to the surface, such as subsurface predators (Safina & Burger 1985, Goyert et al. 2014) or physical forcing (Frank 1992, Schwemmer et al. 2009, Cabot & Nisbet 2013). Clearly, physical aspects of the environment are potentially important for both species.

We investigated the importance of these processes during the summers of 2014 and 2015 at a tern colony on Great Gull Island (GGI), New York, USA, using a radar mounted on the island to observe the birds and a boat-mounted hydroacoustic system to map the distribution of their prey and measure water currents. Radar has several advantages for seabird studies compared to more common techniques like visual observations and telemetry tags. It can locate feeding flocks, and even individual birds, at ranges up to several km. It also does not require attaching anything to the birds, a particular advantage with small seabirds such as terns. While radar reflections from birds can sometimes be masked by 'sea clutter' (i.e. reflections from waves), this interference can also be informative, giving clues as to how water interacts with submerged topography (Bell 1999, Ruessink et al. 2002). Acoustic methods have similar advantages and tradeoffs compared with traditional fish-sampling methods such as nets: they can rapidly sample large volumes of water at high resolution, at the cost of detailed information on the identities of the surveyed animals.

Starting from the general context outlined above, this study was motivated by 2 initial observations made early in the summer of 2014. The first was that tidal rips near GGI were visible to the radar, with shapes and locations that were similar from one tidal cycle to the next. The second was that terns consistently formed feeding flocks in certain locations, which seemed to be associated with the tidal rips. We had several objectives. The first was to precisely map the locations of all feeding flocks, using the radar data. The second was to infer what physical or biological processes made these areas favorable for tern foraging. Finally, we wished to develop a quantitative model that would allow us to predict potentially important tern foraging areas based on physical and bathymetric features.

MATERIALS AND METHODS

Study site and field schedule

Great Gull Island, located at 41° 12′ 7″ N, 72° 7′ 5″ W (Fig. 1A), is home to one of the largest tern colonies in the Northwest Atlantic, with approxi-

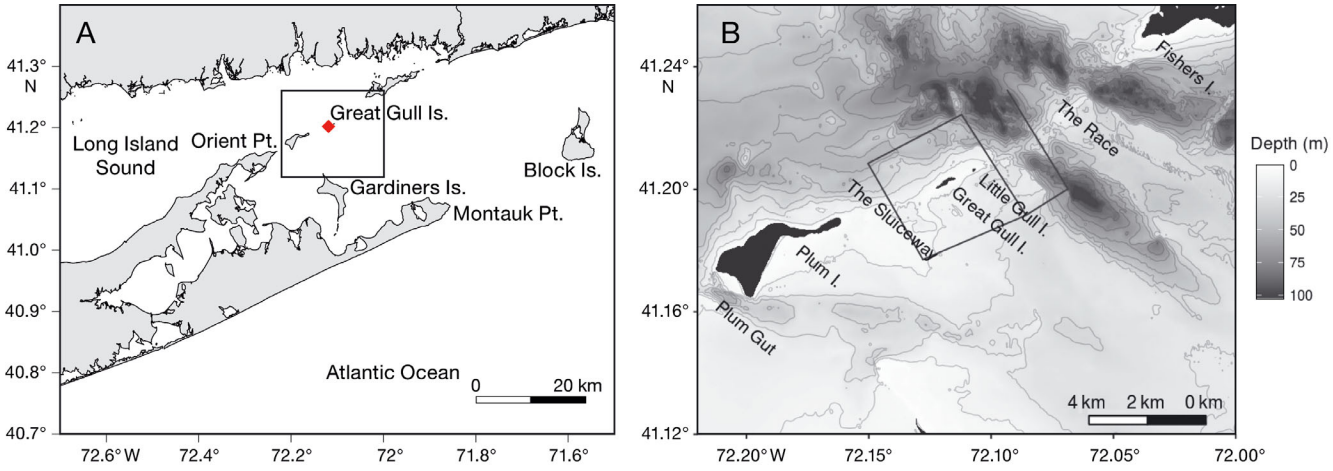

Fig. 1. (A) Eastern Long Island, New York, USA, showing the location of Great Gull Island (GGI) and other landmarks. GGI is located in the center of the Race, a tidal channel connecting Long Island Sound to the Atlantic Ocean. The box around GGI indicates the area shown in (B). (B) Bathymetry of the area surrounding GGI. Contour lines (in grey) are at 10 m intervals. GGI and Little Gull Island are located on a glacial moraine which forms a shallow sill across the mouth of Long Island Sound. Black lines show the acoustic survey transects. This and all subsequent maps are oriented with north up

mately 10 000 breeding pairs of common terns and 1000 pairs of roseate terns. GGI is currently operated by the American Museum of Natural History (AMNH) as a research station. Terns begin to arrive at the island from their wintering grounds in South America in April. They lay eggs starting in late May, and chicks hatch about 21 d later, with the peak hatch in late June. Parents make multiple foraging trips per day to provision their chicks. Both species are single-prey loaders, meaning that they provision their chicks with 1 prey item at a time. Chicks begin to fledge about 24 d after hatching (Cabot & Nisbet 2013), and the birds depart the island to stage for migration in mid- to late August.

The island is located in the center of the Race, the channel connecting Long Island Sound to the Atlantic Ocean (Fig. 1B). The Race is named for its fast currents, which can reach speeds of over 3 m s^{-1} where they flow over the shallow sill at the eastern end of the sound (Fig. 1B). Several channels cross this sill. Between Orient Point and Plum Island is Plum Gut, between Plum Island and GGI is the Sluiceway, and between Little Gull Island (LGI) and Fishers Island is the main channel of the Race. For brevity, we will mostly refer to the entire area collectively as 'the Race' unless we are referring to one of the channels specifically.

Currents in this area are predominantly forced by barotropic pressure gradients due to the semidiurnal tides, which have a typical range between 0.6 and 1.1 m at GGI. The strong mixing due to these tidal currents ensures that the water column in the eastern sound is never more than weakly stratified (O'Donnell et al. 2014). The subtidal currents are typical of an estuary, flowing in at depth along the Connecticut shore and out at the surface along the north shore of Long Island, at average speeds of about 25 cm s^{-1}. (O'Donnell et al. 2014).

We conducted field work on GGI during the summers of 2014 and 2015. We made radar and visual observations on the island approximately every other week from June through August in each year. In addition, 4 acoustic surveys were run from an outboard-powered boat around the island each summer, measuring distribution of the terns' prey using scientific echosounders. In 2015, we also measured the velocity of currents using an acoustic Doppler current profiler (ADCP).

Radar data and ground truth

The radar used in this study was a 25 kW commercial marine radar (Furuno FR-7252), operating in the X-band with a wavelength of 3.2 cm. The radar was operated in horizontal scanning mode, using the stock slotted-waveguide bar antenna, with a horizontal beam width of 1.2° and a vertical beam width of 22°. One radar sweep was digitized every 4.8 s, using a PicoScope 3405B (Pico Technology). We operated the radar in short-range mode, with a pulse length of 0.08 µs giving an effective range resolution of 12 m. Details of the radar system are given by Urmy & Warren (2017).

We operated the radar for at least 1 full day during each week of field work on GGI. These full days began at 04:00 h local time, approximately 1.5 h before sunrise, as the first birds began to depart the island. They ended approximately 2 h after sunset around 22:00 h, by which time most of the birds had returned to the colony. Additional radar data were collected at other times when logistics and weather allowed, including partial days and several overnight runs. The radar was not run when winds were higher than approximately 3 m s^{-1}, since sea clutter due to wind waves became too high. The radar was also not run during rain, since radio waves in the X-band are scattered strongly by raindrops (Larkin & Diehl 2012). Every 30 min while the radar was operating and the sun was above the horizon, we performed a 360° scan of the waters around the island with 8 × 40 binoculars with a built-in compass. During these scans, we noted the presence of any flocks of feeding terns and recorded the estimated number of birds in the flock as well as its compass bearing. Approximately 460 h of radar data were collected over both summers.

After the conclusion of field work, we located each visually confirmed tern flock in the radar data, manually selecting it, calculating its centroid location, and integrating its total backscattered energy. Each flock's total backscattering cross-section was converted to an estimated number of birds using an empirical estimate of the radar cross-section for individual terns and a modified version of the radar equation (Urmy & Warren 2017). The radar's maximum detection range for flocks depends on their size and the level of background clutter, and is not known absolutely. In practice, this range was limited by our ability to ground-truth flocks through binoculars rather than the radar. In fact, flocks were often identified on the radar before being confirmed visually. Within about 4 km of the island, the detection rate for flocks was close to 100%.

Analysis of flock numbers

We counted the number of flocks observed in each half-hourly scan. We then calculated the mean number of flocks, as well as the average number of birds in those flocks, at several levels of aggregation. The coarsest level of aggregation was by year and month, examining inter-annual changes and any changes that might correspond to breeding phenology. In addition, we examined the overall frequency distribution of flock sizes (in number of birds). Preliminary examination showed that the histogram of flock sizes was extremely skewed, and possibly power-law distributed. Power laws can emerge from self-organizing or self-reinforcing processes (Barabási & Albert 1999). Local enhancement of feeding flocks (Pöysä 1992) could be one such process. However, power law distributions are often mis-identified when other distributions are not considered as well (Edwards 2011, Stumpf & Porter 2012). We thus modeled the distribution of flocks sizes using 3 continuous parametric distributions: the Pareto (power-law), gamma, and log-normal. These were fit to the raw data by maximum likelihood, using the R package 'fitdistrplus.' Their goodness-of-fits were compared using Akaike's information criterion (AIC, Akaike 1974).

Acoustic surveys

Survey design and instrumentation

Acoustic surveys used a combination of systematic transects and opportunistic sampling underneath tern feeding flocks when they were present. In both years, these transects included a box centered on GGI, 3.5 km on each side, with the 2 sides east and west of GGI parallel to the direction of tidal flow throughout the Race, and the 2 sides north and south roughly perpendicular to the tidal currents (Fig. 1B). In 2014, an additional transect parallel to the currents was run farther to the east. In 2015, this eastern transect was replaced with a set of short transects closer to the island, targeting several areas identified during the first summer as regular locations for tern feeding flocks.

Four surveys were conducted in each year, timed to coincide with major phases of the breeding season. The first survey in each year took place during the nesting and egg-laying period (31 May 2014, 4 June 2015). The second (10 June 2014, 19 June 2015) occurred during the incubation period, and the third (1 July 2014, 30 June 2015) near the peak hatching date. The final survey, on 22 July in both years, fell towards the end of the chick-rearing phase. Surveys started around 08:00 h local time and concluded between 13:00 and 14:00 h. Surveys took place during both ebb and flood tides on different days, although most surveys also included a change of tide at some point during their ~6 h duration (see Figs. S1 & S2 in the Supplement at www.int-res.com/articles/suppl/m590p227_supp.pdf).

The 2014 surveys were run from a 6.4 m, center-console skiff. In 2015, we used Stony Brook Univer-

sity's RV 'Steinbítur,' at 7.6 m slightly larger and with an enclosed cabin. On both survey craft, the acoustic instruments were deployed on a pole mount over the side at depths between 0.5 and 0.75 m, depending on sea state and the amount of bubble sweepdown.

The acoustic instruments in both years included a 3-frequency echosounder system (38, 120, and 200 kHz) and, in 2015, a 600 kHz ADCP. The echosounder system consisted of a Simrad ES60 38/200 kHz transceiver transmitting through a combined single-beam transducer (model 38/200 Combi-D) and a 120 kHz Simrad ES60 with a split-beam transducer (model ES120-7C). Acoustic beamwidths were 13° × 21° at 38 kHz, and 7° × 7° at 120 and 200 kHz. These echosounders were calibrated using a 38.1 mm tungsten carbide standard target (Foote et al. 1987). All transmitted with a peak power of 1000 W and a pulse length of 0.256 ms (38 kHz), and 0.064 ms (120 and 200 kHz). All echosounders were operated at a ping rate of 2 Hz, corresponding to horizontal ping spacing of 1–1.25 m at typical survey speeds of 2–2.5 m s^{-1}, although the cone-shaped beams overlapped substantially at deeper depths. The ADCP used in 2015 was a 600 kHz Teledyne RDI WHR600. The ADCP was configured to collect velocity information in 1 m depth bins, averaged in 10 s ensembles. At this resolution, the average absolute velocity error was 0.75 cm s^{-1}. Power for all acoustic instruments was supplied by a pair of 12 V marine batteries. Issues with the power supply during the first survey of each year prevented us from operating the 120 kHz echosounder on these dates.

Echosounder data analysis

Echosounder data were processed using Echoview version 7 (www.echoview.com, Myriax). We manually inspected the echograms from all surveys, correcting the bottom detection where necessary and excluding areas of bad data (e.g. engine noise, acoustic cross-talk, bubble sweepdown). The DC power supply was electrically quiet, and noise levels were mostly low on all frequencies. Occasional interference on the 200 kHz echosounder was eliminated using Echoview's 'impulse noise removal' operator.

One of the most important processing tasks was to identify and remove echoes from surface bubble plumes, which were often present in the tidal rips and were the main source of non-biological backscatter. Bubble plumes were removed using a combination of objective and subjective criteria. The objective filter was based on the acoustic characteristics of bubble clouds, which reverberate more strongly at 38 kHz than at higher frequencies due to resonant scattering (D'Agostino & Brennen 1988). We calculated the difference between mean volume backscattering strength (S_v, MacLennan et al. 2002) at 38 and 200 kHz and identified voxels where 38 kHz S_v was higher. These 2 frequencies were used because they were expected to show a large difference for bubble plumes and were available in all 8 surveys. The 38–200 kHz difference was used to define a binary mask of possible bubble areas. A 3 × 3 pixel erosion filter was applied to this mask, followed by a 3 × 3 dilation filter, to eliminate small echoes such as those from individual fish. A second binary mask was created for areas where 38 kHz S_v was higher than −60 dB re m^{-1}, since bubble plumes were expected to scatter strongly. The union of these 2 masks was used to define likely regions of bubble plumes, which were then dilated by 1 ping horizontally and 3.75 m vertically to ensure that the entire plume was identified.

Because bubble plumes share acoustic characteristics with some biological scatterers, such as schools of swimbladdered fish, we did not apply the frequency-differencing-based filter to the entire acoustic record. Instead, we manually defined 'bubble candidate' regions in Echoview, and only applied the filter inside them. These regions were defined in sections of the cruise track where tidal currents ran fast, giving rise to rough water or visible convergence zones on the surface, and where vertically oriented features of elevated S_v were visible extending down from the surface on the echograms. Any of the scattering features in the 'bubble candidate' region which met the criteria of the objective bubble feature were excluded from further analysis. This approach let us confidently eliminate bubble scattering, without having to exclude biological echoes such as subsurface fish schools.

Following denoising and removal of bubble plumes, the survey trackline was partitioned between the planned, systematic transects and the opportunistic sampling underneath feeding flocks. Acoustic data were integrated in cells 1 m deep and 10 m in length and exported from Echoview for further analysis.

We did not sample subsurface prey directly. This constrained our analysis of the acoustic data, although indirect observations allowed us to make some limited interpretations. Because terns deliver 1 whole fish at a time to their young, it was possible to get an estimate of their diet by counting different prey items as birds returned to the colony with them. The terns consumed a variety of small fishes (~3–10 cm in length), predominantly sand eels, young-of-

year clupeids, and American butterfish *Peprilus triacanthus*. Of these, all but sand eels possess gas-filled swim bladders. Several exploratory zooplankton tows in 2014 turned up mostly small (<1 mm) calanoid copepods. Finally, larger swimbladdered fishes such as striped bass *Morone saxatilis* and bluefish *Pomatomus saltatrix* are known to be present in the water column and are the targets of local recreational fisheries (Safina & Burger 1985, 1988).

Using acoustic theory and published models, we predicted the approximate backscattering cross-section σ_{bs} of each of these classes of animals at each acoustic frequency. The backscattering cross-section, measured in m^2, indicates how strongly an object reflects sound, and is used to convert volumetric backscatter measurements to animal densities (Simmonds & MacLennan 2005). Since the σ_{bs} of different scatterers can vary over many orders of magnitude, they are often reported in logarithmic form as target strengths (TS), measured in decibels referenced to 1 m^2 (MacLennan et al. 2002).

For the purposes of acoustic scattering, copepods can be approximated as fluid-like deformed cylinders and modeled using techniques such as the distorted-wave Born approximation (DWBA, Stanton et al. 1998). We used a generic copepod model available in the open-source SDWBA.jl package (Urmy 2016). Sand eels can also be approximated by the DWBA. We used a tapered-cylinder model for a 7 cm sand eel (a typical length) with material properties measured for the closely-related Japanese sand eel *Ammodytes personatus* (Yasuma et al. 2009). This model is also included in the SDWBA.jl package. The other fish species require a different approach, since their echoes are dominated by their gas-filled swim bladder. This was approximated by a prolate-cylinder model (Furusawa 1988), as implemented by Lavia et al. (2016). We calculated backscatter for a small fish with a swimbladder 10 × 2 mm (major × minor ellipsoidal axes), and for a large fish with a swimbladder 6 × 1.5 cm.

Predictions from these models were used to define frequency-difference windows to classify scattering on different regions of the echograms. We focused on differences in TS, and hence volume scattering, between 38 and 200 kHz ($\Delta_{38\text{-}200}$), since these frequencies were available on all survey dates. Predicted zooplankton TS was weak at all frequencies, but was 28 dB higher at 200 kHz, implying an equivalent difference in S_v. Sand eels and small swimbladdered fish had similar values of $\Delta_{38\text{-}200}$, between 5 and 7 dB. Based on these differences, regions with $S_{v,38} - S_{v,200} < -15$ dB were classified as 'zooplankton', and all other areas with S_v above a −80 dB threshold were classified as 'fish.' The prey brought back to the colony was approximately half sand eels. This proportion does not necessarily reflect their relative abundances in the water, but in the absence of better information, we averaged (in the linear domain) the TS values for sand eels and small swimbladdered fish. This gave a 'representative' TS for small, schooling fish of −55 dB at 38 kHz and −49 dB at 200 kHz, with the recognition that there is substantial uncertainty inherent in these numbers.

For all echogram regions classified as fish, numerical densities (n), in fish m^{-3}, were estimated as

$$n = 10^{(S_V - TS)/10} \quad (1)$$

We calculated the density at each frequency using the appropriate TS value, and then took the average across all 3 as the final value. These densities were then integrated over the surface layer, from 0–5 m, and over the remainder of the water column, from 5 m to the bottom. The surface value was intended to represent the prey density available to the terns. Although 5 m is deeper than they are thought to dive, by including slightly deeper waters in this zone we reduced the sampling variability, and there was no indication of shallow stratification or other patterns that could have biased our density estimates.

To obtain an estimate of the abundance of predatory fishes, we also analyzed the acoustic data for larger single targets. We extracted targets from the 38 kHz echogram using the single-target detection (single-beam method 2) operator in Echoview a pulse-length determination level of 6 dB for normalized pulse lengths of 0.5–2.0 and a TS threshold of −45 dB re 1 m^{-2}. This TS cutoff was chosen to select fishes larger than those eaten by the terns. Counts of targets were converted to numerical densities (fish m^{-3}) based on the beam angles and sampled volume at each depth.

Analysis of tidal currents

Timing of tidal phases

Because currents in the Race are tidally dominated, our analysis of the currents around GGI is organized by tidal phase. Data collected in the field (e.g. acoustic transects, radar observations) were classified as taking place during flood, ebb, or slack tides based on tidal current tables published by the National Oceanic and Atmospheric Administration (NOAA) Center for Operational Oceanographic Pro-

ducts and Services (CO-OPS). Current predictions were available at 30 min intervals for a location just southwest of GGI (Station LIS1010, 41.1944° N, 72.1336° W, http://tidesandcurrents.noaa.gov/noaacurrents/Predictions?id=LIS1010_17). The model was calibrated by NOAA using a moored ADCP. Their standard error in terms of speed is approximately 14 cm s^{-1}. Errors in timing of tidal phase were 7 min or less (NOAA National Ocean Service 2016). Events were classified as occurring during the flood if the velocity was greater than 50 cm s^{-1}, and as ebb if the velocity was less than −50 cm s^{-1}. If the absolute value of the velocity was less than 50 cm s^{-1}, the event was considered to take place during slack tide. Using this conservative definition, slack tides in the Race lasted about 1 h, although in actuality, the periods of stationary water were considerably shorter, and the characteristic tidal rips appeared as little as 15–30 min after the tide's turn. A large majority (85%) of flocks occurred during the flood or ebb tide, and the distribution of flocks at slack water was a mix of their flood and ebb distributions. For these reasons, we mostly ignored the slack tide and focused on times when the current was flowing strongly.

We also wished to produce realistic maps of current fields during the flood and ebb tidal phases, for use in interpreting the locations of tern feeding hotspots. Representative current fields for flood and ebb tides were obtained by statistically blending our ADCP measurements with output from the Northeast Coastal Ocean Forecast system (NECOFS, Beardsley & Chen 2014), a high-resolution numerical model of the coastal ocean off the northeastern US. A digital elevation model (DEM) of local bathymetry (Eakins et al. 2009) was available at much higher resolution than that of the NECOFS model (1/3 arc-second, or approximately 10 m, vs. 1 km or more for the NECOFS mesh). Before using the modeled currents to interpret the locations of tern flocks, we interpolated both the currents and the DEM to a uniform grid of square cells 75 m on a side. Finally, we corrected the current field to ensure conservation of mass as the water flowed around local small-scale bathymetric features. The final output of this analysis was an average current field for peak flood and ebb tide in the area surrounding GGI. The current field's features are consistent from one tidal cycle to the next, although the magnitude of the currents increases 30–40% between the neap and spring tides. The details of the interpolation and downscaling are given in the Supplement.

The last step in the analysis of the tidal currents was to calculate 2 derived variables from the interpolated, corrected current fields. The first was simply the scalar current speed at each location. The second derived quantity was the divergence,

$$\mathrm{div}(\mathbf{u}) = \frac{\partial u}{\partial x} + \frac{\partial v}{\partial y} \quad (2)$$

where $\mathbf{u} = (u,v)'$ is the current velocity vector. We approximated the partial derivatives in Eq. (2) with first-order centered differences on the final gridded current fields. Divergence represents the net flow in or out of a local area. Positive divergence at the surface implies upwelling from below, and negative divergence (i.e. convergence) implies downwelling.

Comparison of flock and non-flock areas

From the full set of survey tracks, we selected each of the pre-planned box transects and each opportunistically sampled area beneath a feeding flock. For each transect and flock, we calculated a mean value for each of a number of habitat variables, and then compared their values between the systematic transects and the feeding flocks. These variables included the acoustically-estimated prey density in the upper 5 m of the water column, the minimum depth at which the fish density rose above 1 m^{-3}, and the density of predators (i.e. single targets >45 dB TS) in the upper 10 m. Other variables were the depth of the bottom and the absolute value of its gradient (i.e. the slope), the current speed, the vertical component of the current, and the standard deviation of the vertical current.

For each of these potential habitat variables, we tested whether its mean along the transects was significantly different ($p < 0.05$) from its mean underneath flocks. Because the data for most of the variables were non-normal, we used non-parametric Mann-Whitney *U*-tests.

Statistical model of flock occurrence

In order to better understand the distribution of feeding hotspots, and to attempt to predict their locations in other coastal areas, we built a statistical model for the occurrence of feeding flocks. Flocks were modeled as a spatial point process. The domain around GGI was divided into square grid cells, matching the resolution of the interpolated current variables and bathymetry, and the number of flocks whose centroids fell within each grid cell during each tidal phase were tabulated. The number of flocks in the i^{th} grid cell could then be modeled as a Poisson

variable whose intensity parameter λ_i was a function of the length-m vector of covariates $\boldsymbol{x}_i$ in that cell. We fit this model using a generalized linear model (GLM) with a log-link. If y_i is the number of flocks occurring in cell i, this model is defined as

$$y_i \sim \text{Poisson}(\lambda_i) \quad (3)$$

$$\log(\lambda_i) = \log(a) + \beta_0 + \sum_{j=1}^{m} \beta_j x_{i,j} \quad (4)$$

where β_0 is the intercept, $x_{i,j}$ is the j^{th} of m explanatory variables in the i^{th} cell, and β_j are the regression coefficients. We also included a constant offset a, equal to the area of each grid cell multiplied by the total number of hours that cell was surveyed by the radar. This offset corrected for the fact that the total observation time was greater during ebb tides than flood tides (98 vs. 80 h), and put the response variable λ in convenient units of flocks km^{-2} h^{-1}. The model was fit on a rectangular domain around GGI, between longitude 72.175° and 72.05° W, and latitude 41.16°, 41.24° N.

Several independent variables were available as predictors. These included the bottom depth (in negative meters, with 0 at the surface) and the magnitude of the bottom gradient (i.e. its slope, in degrees), as well as the current speed (in m s^{-1}) and its divergence, with units of s^{-1}. These variables were intended to capture the hypothesized relationship between tidal flow and flock locations. We included each of these variables by itself, as well as all 2-way interactions between them.

The final variable used was distance from the colony, measured in meters from the radar, which was located near the center of the island. This was included for 2 non-mutually exclusive reasons. First, distance could be biologically important. Terns might prefer to forage close to the colony, reducing the time and energy spent commuting. Alternatively, if prey close to the colony become depleted (i.e. 'Ashmole's halo,' Ashmole 1963), they might prefer to forage farther away. Second, the probability of detecting a flock — both visually and with the radar — is expected to decrease at ranges greater than 4–5 km. Including distance from the radar should allow the model to account for this effect separately from the other explanatory variables. To make sure our explanatory variables were not overly collinear, we calculated the Pearson product-moment correlations between them. These correlations were mostly weak, with the strongest between distance and depth, and between depth and slope, both with values of −0.49 (Table 1). This reassured us that the covariates were adequately independent.

Table 1. Explanatory variables for the spatial model were not strongly correlated. Table shows Pearson product-moment correlations between each pair of covariates

	Depth	Slope	Speed	Divergence
Distance	−0.49	0.26	0.036	0.01
Depth		−0.49	0.254	−0.01
Slope			−0.00	−0.01
Speed				−0.03

An ultimate goal of modeling foraging hotspots near GGI is to be able to predict them elsewhere. While bathymetric data are available for most coastal areas, detailed data on currents may not be. We thus fit 2 simpler models without any current variables: one including only depth, slope, and their interaction (in addition to distance and the offset log(a)), and a null model with only distance and the offset. Finally, to evaluate the relative importance of current variables and bathymetry, we fit a model including distance, the offset, current speed, and divergence, but not depth or slope. We compared the fit of the 4 models in an information-theoretic framework (Anderson & Burnham 2002). This approach differs from traditional null-hypothesis significance testing in that it simultaneously compares several models to the available data using AIC, with the goal of identifying the most parsimonious model of the candidate set. The high sample size resulting from the high-resolution spatial grid meant that nearly all combinations of predictor variables were 'significant' at the $p = 0.05$ level. In this context, comparing a few alternative models makes more sense than trying to identify the best model by stepwise regression (Whittingham et al. 2006). To compare the models, we calculated the AIC value for each. We also calculated the 'Akaike weight' (Anderson & Burnham 2002), which estimates the probability that each model in the set would be selected as the best if a replicate dataset drawn from the same process were available. We also calculated the proportion of deviance explained by each model (analogous to R^2 for a normal regression).

RESULTS

Measurements of feeding flocks

Flocks were more numerous in 2014, with an average of 2.1–2.4 flocks observed per half-hourly scan, compared to 1.3–1.6 flocks scan^{-1} in 2015. However, the average size of flocks was larger in 2015 at 118

Table 2. Summary statistics of tern feeding flocks by year and month. The columns give the total number of scans and flocks, as well as the average numbers of flocks scan^{-1}, birds flock^{-1}, the total number of birds feeding in flocks, and the mean distance of flocks from the radar

Year	Month	Scans	Flocks	Flocks scan^{-1}	Birds flock^{-1}	Total birds	Distance (km)
2014	June	114	258	2.26	75	169	1.12
	July	135	322	2.39	89	213	0.79
	August	61	131	2.15	57	123	0.78
2015	June	51	82	1.61	147	236	1.77
	July	68	107	1.57	187	294	1.35
	August	18	24	1.33	24	32	1.35

birds flock^{-1}, compared with 68 birds flock^{-1} in 2014 (Table 2). The number of flocks observed did not change much from one month to the next, but in both years, their sizes in June and July were significantly greater than in August. In both years, the average distance of flocks from the colony decreased by approximately 400 m between June and July, remaining nearly identical from July through August. The average distance of flocks from the colony was also several hundred meters greater in 2015 than in 2014.

The frequency distribution of flock sizes was dramatically skewed (Fig. 2). The majority of flocks contained between 10 and 100 birds, but a handful were much larger, with up to 1200 birds. The data were best approximated by a log-normal distribution with mean 3.98 and standard deviation 1.08. Next best, trailing the log-normal by 105 AIC units, was a Pareto distribution with shape and scale parameters of 3.67 and 260. The worst fit was provided by the gamma distribution, which trailed the log-normal distribution by 185 AIC units. Its fitted shape and rate parameters were 0.95 and 0.0098.

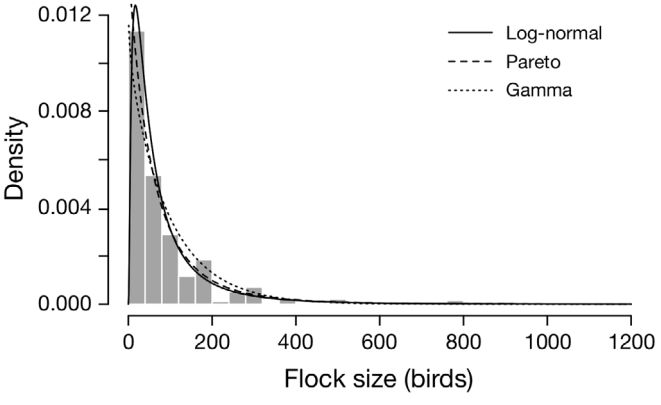

Fig. 2. Frequency distribution of flock sizes (i.e. number of birds) was highly skewed. Bars show the raw data, while the lines show fitted log-normal (solid), Pareto (dashed), and gamma (dotted) distributions. The log-normal distribution provided the best fit to the data

Data collected during the acoustic surveys suggested several differences between the waters beneath flocks and other areas (Fig. 3). Prey were shallower and slightly more abundant under flocks. Large fish were also slightly more abundant under flocks. Average current speeds beneath flocks were 25 cm s^{-1} higher than along the systematic transects. However, none of these differences was statistically significant at the $p = 0.05$ level (Table 3).

There was no obvious spatial trend in the distribution of fishes around GGI (Fig. 4). Integrated water-column values were generally higher along the northern transect, although this was only because the water was deeper there. Overall, fish densities near the surface were low: in 97% of acoustic sampling intervals, the estimated density was <1 fish m^{-2} in the upper 5 m of the water column. When present, however, their densities could be much higher, up to 100 fish m^{-2}. Overall, the areal density of fish in the surface layer was 0.59 fish m^{-2}. The deeper portion of the water column usually contained more fish, with areal densities of 2.3 fish m^{-2} when integrated from 5 m below the surface to the bottom.

Tidal current field

The presence of the islands in the center of the Race forced the water to accelerate and change direction to flow around them. Currents wrapped around both ends of GGI, flowing rapidly close to shore and over the shallowest parts of the Race and Sluiceway (Fig. 5). This led to several well-defined areas of divergence in the velocity field, which shifted depending on the tidal phase (Fig. 6). Some of these areas of divergence, especially off the ends of GGI, seemed to match up with the distribution of average radar clutter and the distribution of flocks (Fig. 7). More water appeared to exit Long Island Sound through Plum Gut and Gardiner's Bay, on the south side of Plum Island, than entered that way during the flood. As a result, currents in the Sluiceway and Race were slightly faster on the flood tide than on the ebb.

During both tidal phases, reflections from patches of rough water were evident in the radar data (Fig. 7). The shape and position of these rough patches

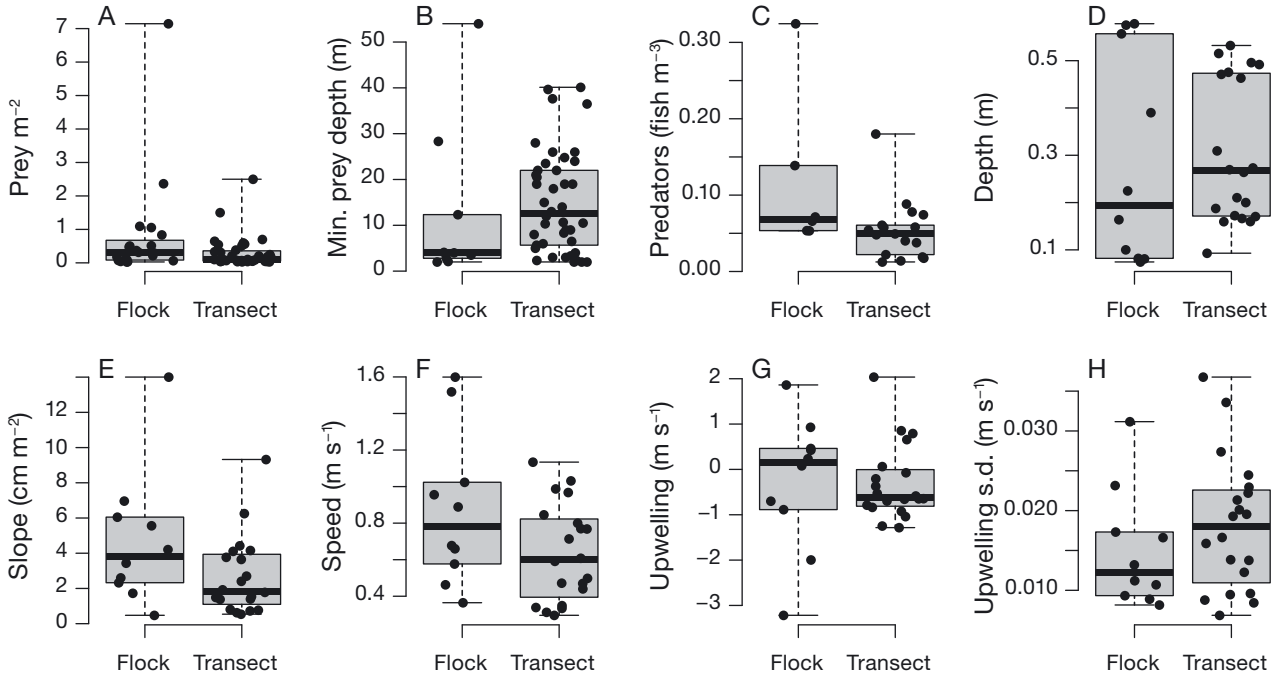

Fig. 3. Mean values of habitat variables underneath each flock and along each systematic transect. Points show the raw data values, with a random horizontal offset added to reduce overplotting. Box plots show the interquartile range and median (horizontal bar); whiskers extend to the total range. The variables are (A) prey density in the upper 5 m, (B) minimum depth of prey fish below the surface, (C) density of large fish in the upper 10 m, (D) bottom depth, (E) bottom slope, (F) horizontal current speed, (G) the vertical component of the current (i.e. up- or downwelling), and (H) variability of the vertical current (standard deviation of the vertical velocity)

Table 3. Habitat variables beneath flocks were not significantly different from those along planned transects. The first 2 columns give the mean value of each variable on planned transects and under flocks. Also shown are p-values for non-parametric Wilcoxon rank-sum tests, along with the total degrees of freedom

Variable	Transect	Flock	p	df
Prey (fish m^{-2})	0.30	0.79	0.15	54
Min. prey depth (m)	15.09	12.58	0.19	49
Predators (fish m^{-3})	0.05	0.12	0.07	21
Bottom depth (m)	0.30	0.28	0.56	28
Bottom slope (cm m^{-1})	2.69	4.74	0.11	28
Current speed (m s^{-1})	0.64	0.87	0.17	28
Vertical current (m s^{-1})	−0.31	−0.28	0.62	28
Vertical current SD (m s^{-1})	0.02	0.01	0.31	28

changed between the flood and ebb, but were nearly identical from one tidal cycle to the next. The ebb-tide pattern included a rough area downstream of the channel between GGI and LGI. It also included a triangular rough patch west of GGI, starting at a point near the western tip of the island and widening to the south. On the flood tide, similar rough patches were present, but to the north side of the islands. One extended west from GGI towards Plum Island. Another started between GGI and LGI, tapering to a point several hundred meters to the north while curving slightly east (Fig. 7). A final patch of rough water, also roughly triangular in shape, extended east into the central Race from LGI. These rough patches were found mostly in areas of convergent flow (Fig. 6). They also appeared to be related to the distribution of tern feeding flocks.

Spatial distribution of flocks

Feeding flocks occurred in different areas depending on the tide (Fig. 8). On the ebb, when the current was flowing out of Long Island Sound, the highest density of flocks was found in a narrow band extending off the western end of GGI, roughly parallel to the isobaths on the northern flank of the shallow sill. Another set of flocks were grouped into a narrow band just north of the shallow channel between GGI and LGI. During the flood, with the current flowing northwest into Long Island Sound, the band of flocks just north of the LGI channel shifted into the center of the channel, equidistant between GGI and LGI. Sim-

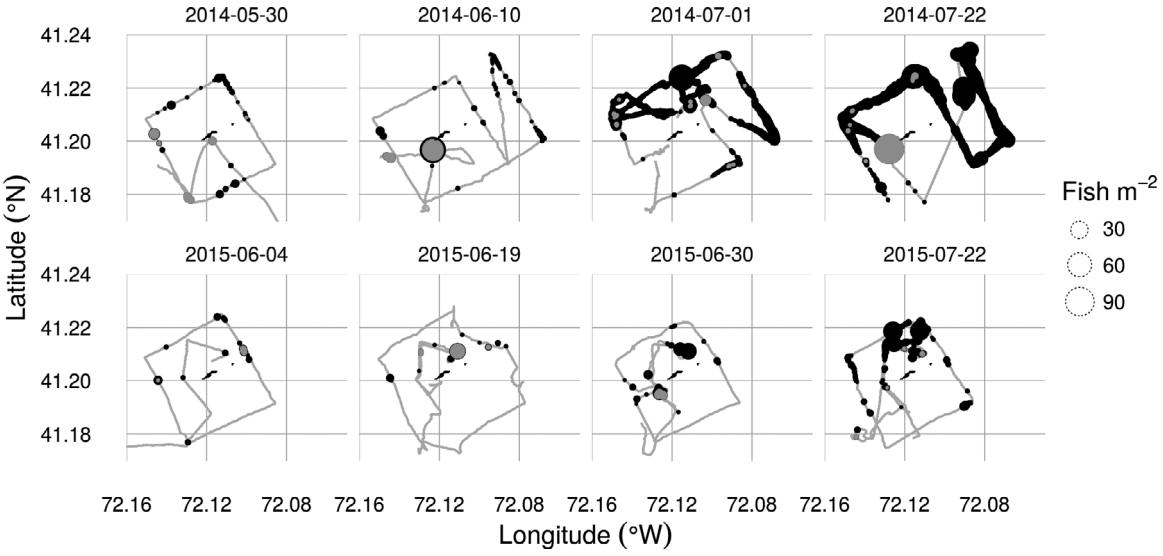

Fig. 4. Estimated density of tern prey, in fish m^{-2}, during the 4 acoustic surveys in 2014 and 2015. These densities were calculated from acoustic backscatter consistent with the small fishes (approximately 3–10 cm in length) which made up most of the terns' diet. Grey line shows the track of the survey boat around Great Gull Island, which is at the center of each plot. The transect box is approximately 3.5 km on each side. The size of the circles is proportional to the density of fish. Black circles indicate the density of fish integrated from the bottom to 5 m below the surface. Grey circles indicate the density of fish in the upper 5 m of the water column

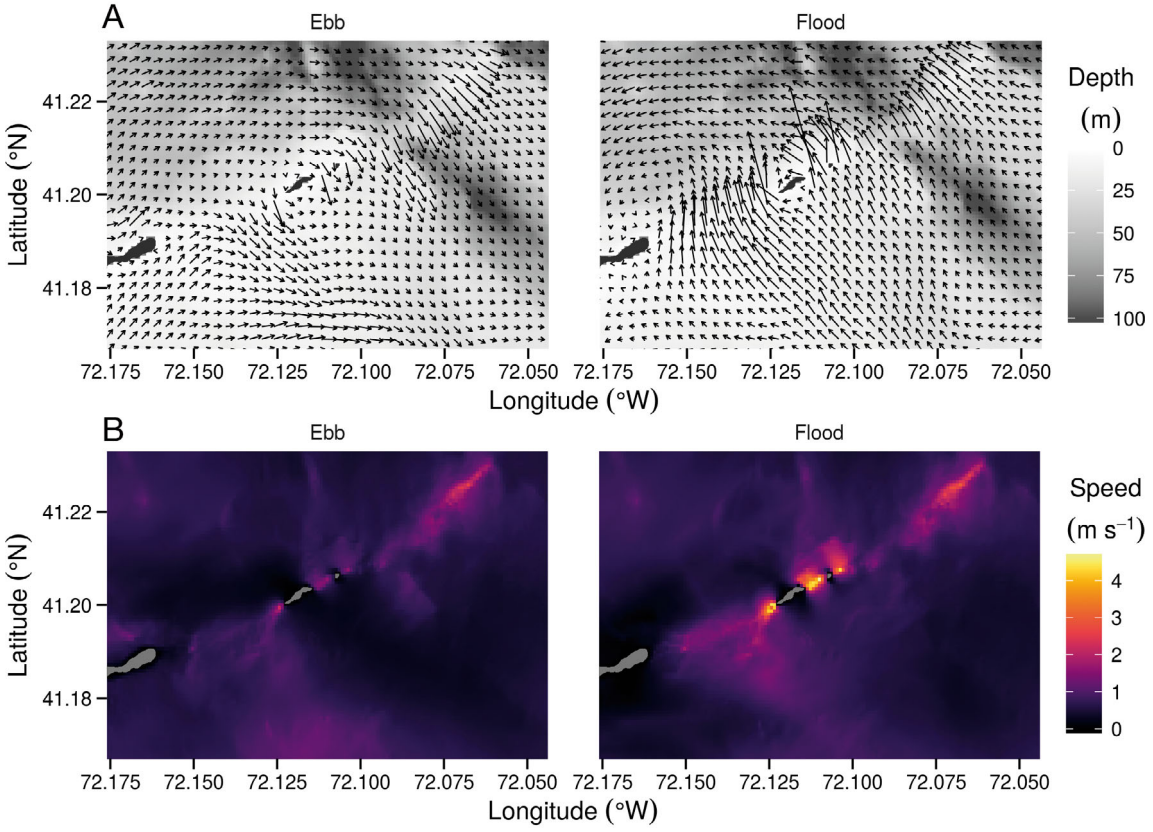

Fig. 5. Tidal currents were fastest over the shallow areas of the Race near Great Gull Island. Left and right panels show average currents at peak ebb and flood tide, respectively. (A) Arrows show the direction of flow over bathymetry (grey shading); length of each arrow is proportional to current speed at that point. (B) Absolute values of current speed. Velocities shown here are water-column averages, based on a blend of acoustic Doppler current profiler (ADCP) measurements and output from the Northeast Coastal Ocean Forecast system (NECOFS) coastal ocean model, and corrected for continuity around the local bathymetry (see 'Materials and methods' for details)

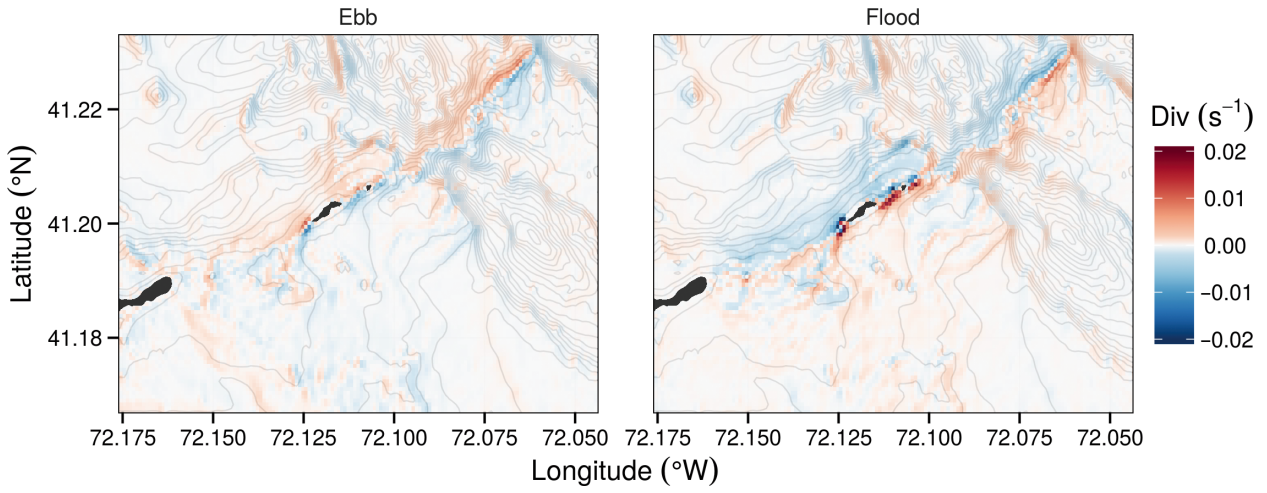

Fig. 6. Tidal flow over shallow bathymetry created distinct areas of diverging and converging currents which shifted position from ebb tide (left panel) to flood (right). Red colors show areas of positive divergence, indicating upwelling, blue areas indicate convergence and downwelling. Contour lines show isobaths at 5 m intervals. Divergence was approximated from the 'analysis' current fields shown in Fig. 5 using spatial finite differences

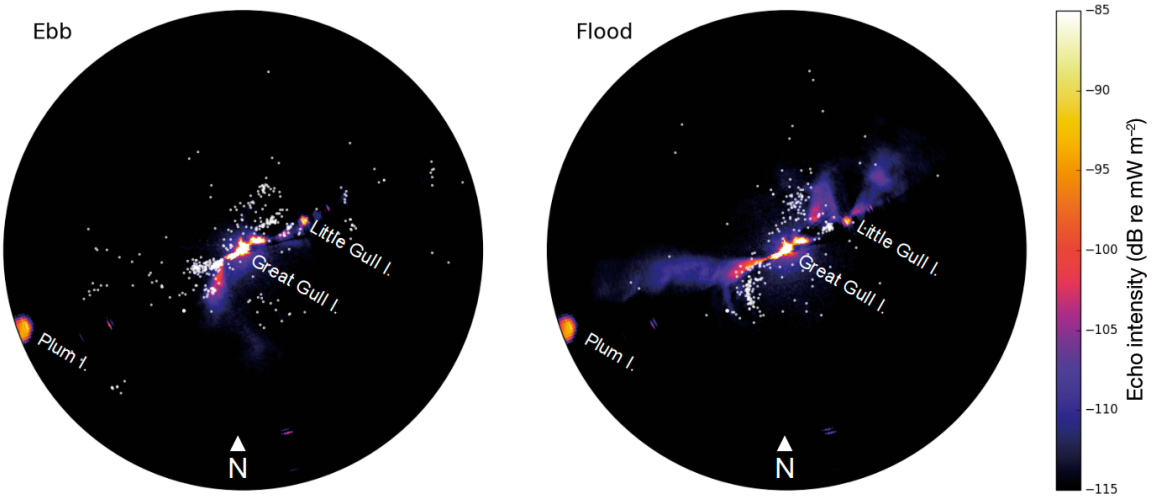

Fig. 7. Radar reflections from sea clutter varied consistently from ebb to flood tidal phases (left and right panels). Colors show average radar echo intensity (in dB re 1 mW m^{-2}) during each tidal phase, and white points show the locations of all tern feeding flocks observed during each tidal phase. The distribution of flocks paralleled some of the radar features, and likewise shifted from ebb to flood. The radius of each subplot is 4 km. Average reflectivity is plotted as raw voltages, and was dominated by scattering from land and the sea surface. The islands shown in Fig. 1B are visible here as the brightest patches, with Great Gull Island at the center, Little Gull Island to the northeast, and the tip of Plum Island at the edge of the circle in the southeast. Larger patches of reflectivity are due to sea clutter. The 'sunburst' around Great Gull Island is due to wind waves, while the extended, wedge-shaped areas of clutter are caused by choppy waves in areas of surface convergence in the tidal rips (cf. blue areas in Fig. 6)

ilarly, off the western end of GGI, most flocks were found farther south than on the ebb tide, in a narrow band starting near the island's western tip and extending west before curving south (Fig. 8). Most flocks were centered over areas of comparatively smooth water just upstream of the rough patches (Fig. 7).

The full statistical model, incorporating bathymetry and currents, was able to describe the distribution of flocks by tidal phase. The modeled flock density was highest in the areas where flocks were most common off the ends of GGI (Fig. 9). It also fitted several smaller, more remote clusters of flocks, such as the flocks occurring over the small bathymetric hump near the edge of the model domain due north of GGI, and the handful over the sill to the northeast of LGI

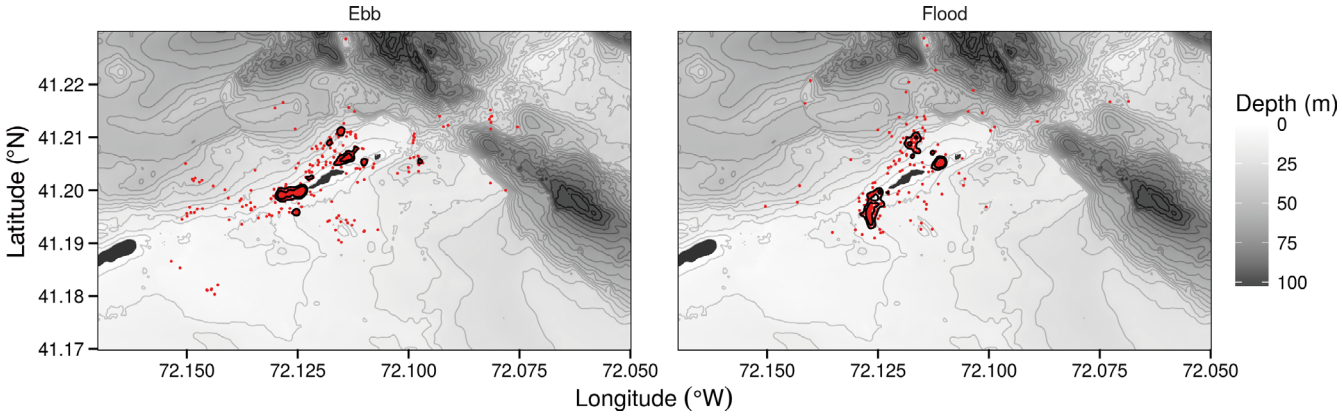

Fig. 8. Locations of tern feeding flocks (points) observed by radar near Great Gull Island, separated by tidal phase. Flocks occurring during the ebb are shown in the left panel, those during the flood on the right. Grey shading shows the local bathymetry; light contour lines are spaced at 5 m intervals. The heavier black contours outline the 75th and 90th percentiles of the kernel density estimate of the flocks' distributions

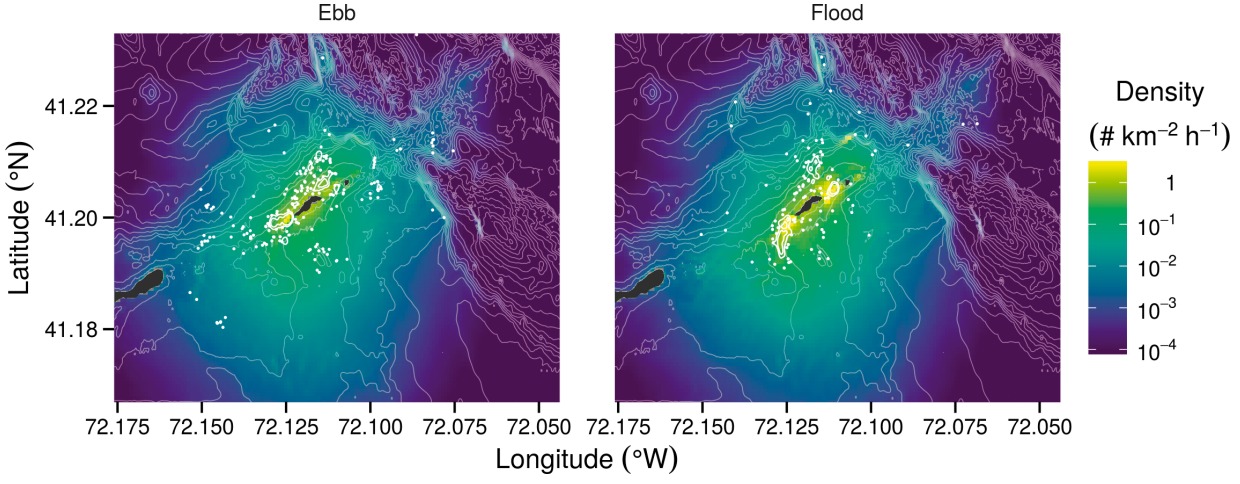

Fig. 9. A spatial regression model was able to capture many of the important features of tern flock distribution near Great Gull Island. Shading shows the density of flocks (number km^{-2} h^{-1}) predicted as a function of depth, bottom slope, current speed, current divergence, and distance from the colony during ebb and flood tides (left and right panels, respectively). White points show locations of real feeding flocks. For visual clarity, flocks are not plotted individually in the densest areas, outlined by heavy white lines. As in Fig. 8, these enclose the 90th and 75th percentiles of the flocks' kernel density distribution. Thin contours show bathymetry at 5 m intervals

(Fig. 9). The full model predicted distinctly different distributions of flocks during flood and ebb tides (Fig. 10).

The coefficients indicated that flocks were more common in shallow water where currents were running fast and diverging (Table 4). All terms in the full model were significant at the p = 0.05 level with the exception of the 3 interaction terms involving depth. In the full model, slope made a positive contribution to flock density, but in the bathymetry-only model, its sign was reversed, probably due to partial correlation with the current variables in the full model. The effect of distance was nearly identical in all 3 models, with predicted density falling off with increasing range.

The full model was unambiguously the best of the 3. It led the next-best current-only model by 170 AIC units, indicating its relative likelihood was $e^{170/2} = 8.2 \times 10^{36}$ greater, and that its added complexity was more than made up for by its better fit to the data. In turn, the current-only model was better than the bathymetry-only model by a similarly large AIC margin (Table 4). The null model did have some explanatory power, accounting for 35% of the deviance. The bathymetry-only and current-only models were better, explaining 40 and 43% of the deviance respectively, and the full model was best, explaining 45% (Table 4).

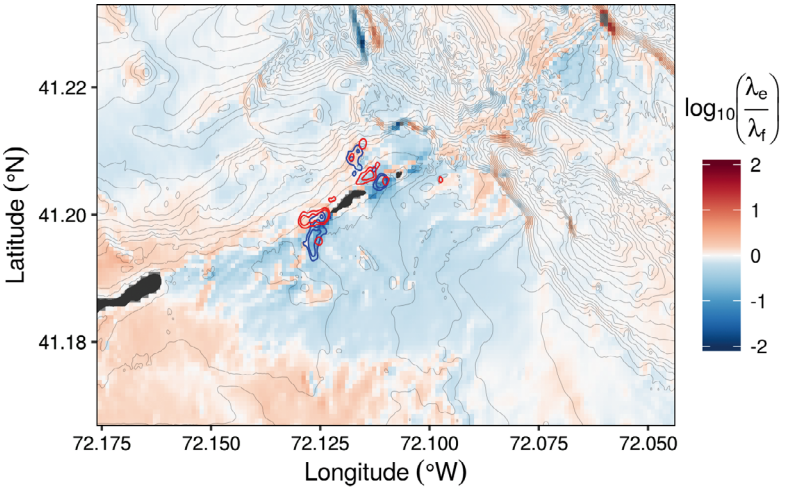

Fig. 10. Areas where flocks were most likely found shifted dramatically between tidal phases. Color scale shows the log-transformed ratio of ebb density (λ_e) to flood density (λ_f). The logarithm used was base-10, so a value of 1, for instance, means that flocks are 10 times more likely on the ebb, while a value of −2 means that they are 100 times more likely on the flood. Blue shading shows areas where flocks are more common on the flood, while red shading indicates that they are more common on the ebb. It is important to emphasize that these are relative, not absolute, densities. Blue and red countours enclose the 90th and 75th precentiles of the observed flocks' kernel density ditributions on the flood and ebb, respectively. Grey contours show bathymetry at 5 m intervals

Table 4. Results of Poisson generalized linear models for flock density. Parameter estimates (Est.) and standard errors are shown for 3 models: a full model including all covariates, reduced models with current or bathymetric variables only, and a null model with only distance from the colony. Lower section of the table gives summary statistics for each model's fit: AIC: Akaike's information criterion, Δ_{AIC}: AIC difference from the best model, and w: the proportion of deviance (Dev.) explained

	Full		Current only		Bathymetry only		Null	
	Est.	SE	Est.	SE	Est.	SE	Est.	SE
(Intercept)	−0.542	0.170	−0.504	0.088	0.856	0.117	0.268	0.067
Distance	−0.002	0.000	−0.002	0.000	−0.001	0.000	−0.002	0.000
Depth	0.058	0.010			0.098	0.007		
Slope	16.840	4.209			−0.745	2.740		
Speed	0.904	0.090	0.776	0.032				
Divergence	314.391	33.072	177.897	20.631				
Depth:Slope	−0.090	0.100			−0.464	0.067		
Depth:Speed	−0.010	0.013						
Depth:Div	−1.194	3.731						
Slope:Speed	−12.856	3.131						
Slope:Div	−3526.844	646.075						
Speed:Div	−60.747	7.318	−49.761	6.408				
AIC		4115.639		4286.086		4462.252		4755.516
Δ_{AIC}		0.000		170.447		346.613		639.877
w		1.000		0.000		0.000		0.000
Dev. explained		0.456		0.425		0.395		0.345

DISCUSSION

Feeding flocks

The consistency of the flock locations during the different tidal phases, as well as the acoustically measured variables and statistical models, suggested that foraging opportunities for terns at GGI are strongly mediated by tidal flow. Preferred foraging areas were in shallow areas near the colony where tidal flow was fastest. This result agrees with prior studies on the habitat preferences of common (Rock et al. 2007a, Schwemmer et al. 2009) and roseate (Rock et al. 2007b) terns. However, thanks to the precise flock locations from the radar, as well as the high-resolution bathymetry and current data available for this area, we were able to go a step further and suggest the physical mechanisms behind this habitat preference. In particular, tern flocks tended to form on the upstream side of shallow areas, where water was forced to accelerate over the topography, leading to divergence. Divergence at the surface implies upwelling from below, which brings small prey items closer to the surface

where they are available to the terns. This mechanism is also consistent with the observation that flocks formed almost exclusively over smooth water, evident in Fig. 7 as areas of low sea clutter. Water that is actively upwelling often appears smooth if comes to the surface faster than wind can create capillary waves (Larson & Wright 1975). The absence of waves may also be an advantage for the terns if it makes it easier to see subsurface prey from the air. In this light, it makes sense that divergence was the strongest predictor of flock locations.

None of the other measured variables was significantly different between the flock and transect areas. This is likely due in part to the small number of flocks targeted by the survey boat, and a few suggestive differences are worth pointing out, with the understanding that they require further confirmation. The standard deviation of vertical currents was lower under feeding flocks, discounting the hypothesis that enhanced turbulent mixing defined foraging hotspots. Average currents under flocks were 38% faster than along the transects (Table 3). This agreed qualitatively with the regression model, which identified a positive relationship between current speed and flock density (Table 4). As such, we cannot rule out the 'search volume' hypothesis —that the terns take advantage of fast currents to bring more prey to them.

While prey densities below flocks were slightly higher on average than those measured elsewhere, there was substantial overlap in the 2 distributions (Fig. 3), and the difference in means was not significant (Table 3). The acoustic surveys did not show any overall pattern in the locations of near-surface prey. These results are not entirely unexpected. Correlations between seabirds and their prey are often scale-dependent (Fauchald 2009), and may not be apparent when data are analyzed at the finest (e.g. <1 km) scales (Schneider & Piatt 1986, Fauchald & Erikstad 2002, Burger et al. 2004). The density of individual echoes consistent with large fish was also slightly higher under flocks. Terns are known to feed in association with subsurface predators (Safina & Burger 1985, Goyert et al. 2014). This facultative interaction probably does play a role in tern foraging near GGI. However, if it were the primary mechanism bringing prey to the surface, we would expect flocks to be distributed more uniformly in space. Instead, they were clustered in well-defined locations that were clearly related to the interaction of tidal currents with shallow topography. This suggests, at least in this local area, that physical forcing is more important.

Our results suggest that tidal currents enhanced opportunities for foraging but did not concentrate prey or increase their abundance. Based on informal observations from GGI, the rate of active diving could vary widely between flocks. In some flocks, especially large ones, diving was fast and nearly continuous. However, some other flocks persisted for hours, with dozens of terns circling and hovering continuously, but only a few diving to the surface every minute. These facts suggest that high prey density is not necessary to trigger the coalescence of a flock. Instead, they may be initiated by some combination of individual birds' memory or anticipation of good foraging locations and socially self-reinforcing dynamics (e.g. local enhancement, Pöysä 1992). Measuring the relationship between diving rate and flock size could clarify the dynamics of flock formation and would be worth future study.

The picture that emerges is of a foraging environment that is relatively consistent in space, but unpredictable in time. Based on the modeled currents in the Race, a given water parcel should travel on the order of 10 km in and out of Long Island Sound on successive tidal cycles. Fish in the size range eaten by terns maintain swimming speeds on the order of 50 cm s^{-2} (Bainbridge 1957), while currents through most of the Race are 2–8 times faster (Fig. S2b in the Supplement). The terns' prey most likely struggle to control their horizontal position in these currents, so the same population of ichthyoplankton probably drifts through the Race repeatedly. Most may be able to stay out of the upper water column where they are available to the terns, but a few unlucky ones will be brought there by upwelling or turbulent mixing — which is most likely to happen in the flock hotspots, where at least a few terns are usually waiting.

When a dense patch of prey drifts through one of the favorable foraging areas, a large flock can apparently form quickly in response. In this context, the approximately power-law distribution of flock sizes is particularly interesting. One way that power-law distributions can arise is through self-reinforcing cycles, sometimes called the 'rich-get-richer' phenomenon, where the growth rate of some quantity is positively related to the quantity itself (Barabási & Albert 1999). Recruitment of seabirds to existing flocks (i.e. 'local enhancement,' Pöysä 1992, Grünbaum & Veit 2003, Thiebault et al. 2014) could fit this description, since larger flocks are more conspicuous and can attract conspecifics from farther away (Haney et al. 1992).

The flock numbers presented here can also be interpreted in the context of the entire population on GGI. At any given time, 100–300 birds on average

were found in feeding flocks within a few km of GGI — in other words, about 1–2% of the total breeding population of 20 000. The largest flock sizes, between 800 and 1200 birds, represented about 5% of the population, but only 1% of all flocks observed were this large. Many birds tracked with the radar appeared to depart for, and return from, foraging locations beyond its detection range (2–3 km for single birds and at least 4–5 km for flocks, Urmy & Warren 2017), so it is probable that terns from GGI feed in flocks elsewhere as well. It is thus not possible to determine the total proportion of birds which feed in concentrated flocks, as opposed to individually.

The data presented in this paper allow us to make first-order estimates of several important quantities related to the colony's food needs. Based on observations of several nests during 2015, each pair of adult terns delivered approximately 40 fish d^{-1} to their chicks (J. Walsh unpubl. data). Assuming the parents consume a similar number of fish (their actual consumption is unknown, since they feed at sea), each nest requires approximately 80 small fish d^{-1}. Multiplied by 10 000 nests, this makes for an approximate colony-wide daily ration of 800 000 fish. The average areal density of fish in the upper 5 m was 0.5 fish m^{-2}, so the average density in the upper meter would be 0.1 fish m^{-2}, and the daily ration could be supplied by an 8 km^2 patch of average water. Over the course of a 90 d breeding season, the terns could deplete 720 km^2 of surface waters, equivalent to a patch 27 km on a side.

If the terns could dive the full depth of the water column, the density of fish available to them would increase by a factor of 20. The colony's entire daily ration could then be gleaned from a square of water 400 m on a side, and their seasonal needs from a square 6 km on a side. These calculations reinforce the conclusion that terns are not limited by the abundance of fish per se, but by their availability at the surface. (Of course, if fish are more abundant in general, more will end up in the surface zone).

Tidal currents

More than any other aspect of the tidal currents, terns formed flocks over areas of surface divergence. A steady, incompressible current diverges, by definition, in areas where it accelerates. In the Race, this occurs on the upstream side of the shallow sill and around the islands. Here, the reduced cross-sectional area of the channel causes water to pile up on the upstream side until the resulting pressure gradient is strong enough to accelerate the water and re-establish equal flux at all points across the sill. At the time scale of tern feeding — seconds to hours — this average flow is approximately steady, ignoring small-scale turbulence and eddies. This conclusion is supported by the stationary appearance of the tidal rips visible on the radar, which barely changed shape over several hours around peak flood or ebb tide. These features probably represent areas of surface convergence (Farmer et al. 1995).

If tern foraging is as strongly influenced by tidal flow as it appears, the prediction of foraging hotspots in other areas will rely on accurate current fields — although bathymetry alone does have some predictive power, as shown by the intermediate-complexity model. For this purpose, the NECOFS model output was fair, but not excellent. While the model is high-resolution at the scale of the continental shelf, with nodes spaced only a few hundred meters apart, its resolution was too coarse to capture the extremely fine-scale (~10–100 m) features associated with tern feeding. Our continuity-correction procedure appeared to perform well here. It would be simple to apply in other areas to quickly downscale model output if fine-resolution currents were needed to predict tern foraging hotspots. Of course, this model should be confirmed in other areas before being used for applied predictions. In other areas where currents are not as strong as in the Race, other processes (e.g. interactions with subsurface predators) may take on more importance.

Significance and applications

Terns form feeding flocks near Great Gull Island where currents flow upslope and accelerate over shallow areas. The most important aspect of this process appears to be the divergence of water at the surface where it accelerates, presumably because it draws prey up from below. This conclusion is not surprising in light of previous work on seabird foraging, which has often suggested similar ideas (Hunt et al. 1999, Schwemmer et al. 2009). However, these ideas have often been expressed as qualitative explanations or correlative models. To make accurate predictions, understanding the underlying process is critical. The present study, and the methods presented in it, are valuable because they start to reveal these processes.

This study integrates together several different types of remote-sensing data to obtain a more detailed picture of tern foraging than previously avail-

able. In particular, using a radar to measure the distribution of hundreds of flocks in 2 dimensions allowed us to confidently identify feeding hotspots and, with the auxiliary data on currents and bathymetry, reason about the physical processes underlying them. Additionally, the hydroacoustic estimates of subsurface prey density gave perspective on the factors limiting the terns' food supply — namely, that there are plenty of fish in the sea, but not necessarily enough at the surface. When compared with other processes that can bring fish to the surface, such as sub-surface predators (Safina & Burger 1985, Goyert et al. 2014), tidal currents have some important advantages from the point of view of a foraging tern. They are much more predictable and consistent, and unlike subsurface predators, they do not eat the fish while bringing them to the surface (Safina & Burger 1985).

These factors may make islands or beaches near tidal races particularly favorable locations for colonies of terns and other surface-diving seabirds. This hypothesis could be tested by replicating this study at other coastal tern colonies to see if feeding hotspots occur in locations with similar current and bathymetric features. If confirmed, a spatial model such as that presented here could be used to predict likely feeding hotspots based solely on bathymetry and tidal currents, knowledge which could be extremely useful in planning offshore infrastructure projects, such as wind farms, to minimize their impact on terns and other seabirds. This is important, because common and roseate terns are protected to different degrees under federal and state laws in the USA. The number of offshore infrastructure projects in planning or construction is increasing, and their impact on these and other species is a topic of investigation and concern. Our results show how localized and predictable foraging hotspots can be. If these results are obtained elsewhere, relatively minor repositioning of structures might be able to dramatically reduce their impact.

Acknowledgements. We thank Helen Hays of the AMNH and Great Gull Island Project for allowing us to work on GGI. We also thank Captains Andy Brosnan and Brian Gagliardi for operating the survey craft. Chris Powers, Maija Niemisto, Hannah Blair, and Brandyn Lucca also assisted with boat surveys. This project would not have been possible without Maria Anderson, Emily Runnells, and Ana Livia Furtado, who provided invaluable assistance in the field. Joan Walsh shared unpublished data from nest observations in 2015. Ron Larkin, Michael Schrimpf, and Emily Runnels provided comments on various drafts. We are grateful to George Hunt and 2 anonymous referees for their helpful reviews of the manuscript. Funding was provided by the Frank M. Chapman Memorial Fund of the AMNH. This project was approved by the Stony Brook University Institutional Animal Care and Use Committee (application number 2014-2101).

LITERATURE CITED

Akaike H (1974) A new look at the statistical model identification. IEEE Trans Automat Control 19:716–723

Anderson DRB, Burnham KP (2002) Model selection and multimodel inference, 2nd edn. Springer, New York, NY

Ashmole NP (1963) The regulation of numbers of tropical oceanic birds. Ibis 103:458–473

Bainbridge BYR (1957) The speed of swimming of fish as related to size and the frequency and amplitude of the tail beat. J Exp Biol 35:109–133

Barabási AL, Albert R (1999) Emergence of scaling in random networks. Science 286:509–512

Beardsley RC, Chen C (2014) Northeast Coastal Ocean Forecast System (NECOFS). A multi-scale global-regional-estuarine FVCOM model. American Geophysical Union Fall Meeting Abstracts 2014 OS23C-1211

Becker PH, Frank D, Sudmann SR (1993) Temporal and spatial pattern of common tern (*Sterna hirundo*) foraging in the Wadden Sea. Oecologia 93:389–393

Bell PS (1999) Shallow water bathymetry derived from an analysis of X-band marine radar images of waves. Coast Eng 37:513–527

Bridge ES, Jones AW, Baker AJ (2005) A phylogenetic framework for the terns (Sternini) inferred from mtDNA sequences: implications for taxonomy and plumage evolution. Mol Phylogenet Evol 35:459–469

Burger AE, Hitchcock CL, Davoren GK (2004) Spatial aggregations of seabirds and their prey on the continental shelf off SW Vancouver Island. Mar Ecol Prog Ser 283: 279–292

Cabot D, Nisbet I (2013) Terns. Collins, London

D'Agostino L, Brennen CE (1988) Acoustical absorption and scattering cross sections of spherical bubble clouds. J Acoust Soc Am 84:2126–2134

Decker MB, Hunt GL Jr (1996) Foraging by murres (*Uria* spp.) at tidal fronts surrounding the Pribilof Islands, Alaska, USA. Mar Ecol Prog Ser 139:1–10

Duffy DC (1986) Foraging at patches: interactions between common and roseate terns. Ornis Scand 17:47–52

Eakins BW, Taylor LA, Carignan KS, Warnken RR, Lim E, Medley P, Schoolcraft DC (2009) Digital elevation model of Nantucket, Massachusetts: procedures, data sources and analysis. Tech Memo NESDIS NGDC-26. NOAA, Department of Commerce, Boulder, CO

Edwards AM (2011) Overturning conclusions of Lévy flight movement patterns by fishermen and foraging animals. Ecology 92:1247–1257

Farmer DM, Asaro EAD, Trevorrow MV, Dairiki GT (1995) Three-dimensional structure in a tidal convergence front. Cont Shelf Res 15:1649–1673

Fauchald P (2009) Spatial interaction between seabirds and prey: review and synthesis. Mar Ecol Prog Ser 391: 139–151

Fauchald P, Erikstad KE (2002) Scale-dependent predator-prey interactions: the aggregative response of seabirds to prey under variable prey abundance and patchiness. Mar Ecol Prog Ser 231:279–291

Foote K, Knudsen H, Vestnes G, MacLennan D, Simmonds E

(1987) Calibration of acoustic instruments for fish density estimation: a practical guide. ICES Coop Res Rep 144. International Council for the Exploration of the Sea, Copenhagen

Frank D (1992) The influence of feeding conditions on food provisioning of chicks in common terns *Sterna hirundo* nesting in the German Wadden Sea. Ardea 80:45–55

Furusawa M (1988) Prolate spheroidal models for predicting general trends of fish target strength. J Acoust Soc Jpn E 9:13–24

Godø OR, Samuelsen A, Macaulay GJ, Patel R and others (2012) Mesoscale eddies are oases for higher trophic marine life. PLOS ONE 7:e30161

Goyert HF, Manne LL, Veit RR (2014) Facilitative interactions among the pelagic community of temperate migratory terns, tunas and dolphins. Oikos 123:1400–1408

Grünbaum D, Veit RR (2003) Black-browed albatrosses foraging on Antarctic krill: density-dependence through local enhancement? Ecology 84:3265–3275

Haney JC, Fristrup KM, Lee DS (1992) Geometry of visual recruitment by seabirds to ephemeral foraging flocks. Ornis Scand 23:49–62

Haury L, McGowan J, Wiebe P (1978) Patterns and process in the time-space scales of plankton distributions. In: Steele J (ed) Spatial pattern in plankton communities, Vol 3. Springer, Boston, MA, p 277–327

Hunt GL Jr, Harrison NM (1990) Foraging habitat and prey taken by least auklets at King Island, Alaska. Mar Ecol Prog Ser 65:141–150

Hunt GL Jr, Coyle KO, Hoffman S, Decker MB, Flint EN (1996) Foraging ecology of short-tailed shearwaters near the Pribilof Islands, Bering Sea. Mar Ecol Prog Ser 141: 1–11

Hunt GL Jr, Russell RW, Coyle KO, Weingartner T (1998) Comparative foraging ecology of planktivorous auklets in relation to ocean physics and prey availability. Mar Ecol Prog Ser 167:241–259

Hunt GL Jr, Mehlum F, Russell RW, Irons D, Decker B, Becker PH (1999) Physical processes, prey abundance, and the foraging ecology of seabirds. In: Adams NJ, Slotow RH (eds) Proc 22nd International Ornithological Congress. BirdLife South Africa, Durban, p 2040–2056

Irons DB (1998) Foraging area fidelity of individual seabirds in relation to tidal cycles and flock feeding. Ecology 79: 647–655

Johnston DW, Thorne LH, Read AJ (2005) Fin whales *Balaenoptera physalus* and minke whales *Balaenoptera acutorostrata* exploit a tidally driven island wake ecosystem in the Bay of Fundy. Mar Ecol Prog Ser 305:287–295

Kinder TH, Hunt GL, Schneider D, Schumacher JD (1983) Correlations between seabirds and oceanic fronts around the Pribilof Islands, Alaska. Estuar Coast Shelf Sci 16:309–319

Larkin RP, Diehl RH (2012) Radar techniques for wildlife research. In: Silvy NJ (ed) Techniques for wildlife investigations and management, 7th edn. Johns Hopkins University Press, Baltimore, MD, p 319–339

Larson TR, Wright JW (1975) Wind-generated gravity-capillary waves: laboratory measurements of temporal growth rates using microwave backscatter. J Fluid Mech 70:417–436

Lavia E, González JD, Blanc S (2016) A computational method to calculate the exact solution for acoustic scattering by liquid spheroids. arXiv:1603.00499v2, https://arxiv.org/pdf/1603.00499.pdf

MacLennan DN, Fernandes PG, Dalen JD (2002) A consistent approach to definitions and symbols in fisheries acoustics. ICES J Mar Sci 59:365–369

NOAA National Ocean Service (2016) Tidal current prediction error for United States stations. Tech Rep. National Oceanic and Atmospheric Administration. http://tidesandcurrents.noaa.gov/noaacurrents/doc/Tidal_Current_Prediction_Uncertainty.pdf

O'Donnell J, Wilson RE, Lwiza K, Whitney M and others (2014) The physical oceanography of Long Island Sound. In: Latimer JS, Tedesco MA, Swanson RL, Yarish C, Stacey PE, Garza C (eds) Long Island Sound: perspectives for the urban sea. Springer Series on Environmental Management. Springer, New York, NY, p 79–158

Pöysä H (1992) Group foraging in patchy environments: the importance of coarse-level local enhancement. Ornis Scand 23:159–166

Rock JC, Leonard ML, Boyne AW (2007a) Do co-nesting Arctic and common terns partition foraging habitat and chick diets? Waterbirds 30:579–587

Rock JC, Leonard ML, Boyne AW (2007b) Foraging habitat and chick diets of roseate tern, *Sterna dougallii*, breeding on Country Island, Nova Scotia. Avian Conserv Ecol 2:4, http://www.ace-eco.org/vol2/iss1/art4/

Ruessink BG, Bell PS, Van Enckevort IMJ, Aarninkhof SGJ (2002) Nearshore bar crest location quantified from time-averaged X-band radar images. Coast Eng 45:19–32

Safina C (1990) Foraging habitat partitioning in roseate and common terns. Auk 107:351–358

Safina C, Burger J (1985) Common tern foraging: seasonal trends in prey fish densities and competition with bluefish. Ecology 66:1457–1463

Safina C, Burger J (1988) Prey dynamics and the breeding phenology of common terns (*Sterna hirundo*). Auk 105:720–726

Safina C, Wagner RH, Witting DA, Smith KJ (1990) Prey delivered to roseate and common tern chicks; composition and temporal variability. J Field Ornithol 61:331–338

Schneider D, Piatt JF (1986) Scale-dependent correlation of seabirds with schooling fish in a coastal ecosystem. Mar Ecol Prog Ser 32:237–246

Schwemmer P, Adler S, Guse N, Markones N, Garthe S (2009) Influence of water flow velocity, water depth and colony distance on distribution and foraging patterns of terns in the Wadden Sea. Fish Oceanogr 18:161–172

Shealer DA, Kress SW (1994) Post-breeding movements and prey selection of roseate terns at Stratton Island, Maine. J Field Ornithol 65:349–362

Simmonds J, MacLennan D (2005) Fisheries acoustics: theory and practice, 2nd edn. Blackwell Science, Oxford

Stanton TK, Chu D, Wiebe PH (1998) Sound scattering by several zooplankton groups. II. Scattering models. J Acoust Soc Am 103:236–253

Stumpf MPH, Porter MA (2012) Critical truths about power laws. Science 335:665–666

Thiebault A, Mullers R, Pistorius P, Meza-Torres MA, Dubroca L, Green D, Tremblay Y (2014) From colony to first patch: processes of prey searching and social information in Cape Gannets. Auk 131:595–609

Thorne LH, Read AJ (2013) Fine-scale biophysical interactions drive prey availability at a migratory stopover site for *Phalaropus* spp. in the Bay of Fundy, Canada. Mar Ecol Prog Ser 487:261–273

Urmy SS (2016) SDWBA.jl: a Julia package for modeling acoustic backscatter from zooplankton. https://github.com/ElOceanografo/SDWBA.jl

Urmy SS, Warren J (2017) Quantitative ornithology with a commercial marine radar: standard-target calibration, target detection and tracking, and measurement of echoes from individuals and flocks. Methods Ecol Evol 8: 860–869

USFWS (US Fish and Wildlife Service) (1998) Roseate tern *Sterna dougalii* Northeastern population recovery plan, first update. Tech Rep. U.S. Fish and Wildlife Service, Hadley, MA

Warren JD, Santora JA, Demer DA (2009) Submesoscale distribution of Antarctic krill and its avian and pinniped predators before and after a near gale. Mar Biol 156: 479–491

Weimerskirch H (2007) Are seabirds foraging for unpredictable resources? Deep Sea Res II 54:211–223

Whittingham MJ, Stephens PA, Bradbury RB, Freckleton RP (2006) Why do we still use stepwise modelling in ecology and behaviour? J Anim Ecol 75:1182–1189

Yasuma H, Nakagawa R, Yamakawa T, Miyashita K, Aoki I (2009) Density and sound-speed contrasts, and target strength of Japanese sandeel *Ammodytes personatus*. Fish Sci 75:545–552

Zamon JE (2003) Mixed species aggregations feeding upon herring and sandlance schools in a nearshore archipelago depend on flooding tidal currents. Mar Ecol Prog Ser 261:243–255

Zamon JE, Phillips EM, Guy TJ (2014) Marine bird aggregations associated with the tidally-driven plume and plume fronts of the Columbia River. Deep Sea Res II 107:85–95

Editorial responsibility: Keith Hobson, London, Ontario, Canada

Submitted: August 3, 2017; Accepted: December 7, 2017
Proofs received from author(s): February 20, 2018